International Journal of Fluid Power 14 (2013) No. 1 pp. 25-36

TEMPERATURE PREDICTION OF DISPLACEMENT CONTROLLED MULTI-ACTUATOR MACHINES

Enrique Busquets and Monika Ivantysynova

Purdue University, Department of Mechanical Engineering, 225 S. University St., West Lafayette, Indiana 47907, USA
ebusquet@purdue.edu, mivantys@purdue.edu

Abstract

A promising technology for the advancement of fluid power systems is displacement controlled (DC) actuation. The main advantage of DC actuation is that metering losses are completely eliminated by replacing each actuator's proportional valve with a variable displacement pump and controlling the actuator motion by pump displacement. This technology can achieve up to 50 % energy savings when compared to the conventional load sensing (LS) systems and the elimination of metering losses in DC systems is directly translated in lower heat generation. This paper presents a model to predict the thermodynamic behavior of multi-actuator displacement controlled machines. A complete mathematical model has been developed based on conservation of mass and energy. The model characteristics are discussed for an excavator, which contains four variable displacement pumps, three single-rod actuators, a rotary actuator for the slew, a gear pump, an accumulator, a heat exchanger, a reservoir, as well as metallic hydraulic lines and switching valves; however, the model has been created to be able to simulate not only the presented hydraulic circuit but different ones including those for larger off highway vehicles. Simulation results for measured working cycles of the excavator are presented and compared with measured temperatures of the machine. The simulation/measurement agreement demonstrates the validity and usefulness of the model.

Keywords: displacement control, excavator, heat transfer, thermodynamics

1 Introduction

Over the last decades there has been an emphasis on the design of efficient fluid power systems. Although improvements in efficiency of the individual hydraulic components can increase system efficiency to a certain degree, the demand for higher system efficiencies has driven researchers to investigate alternatives to the traditional valve controlled actuation. A promising technology for the improvement of fluid power systems efficiency is displacement controlled (DC) actuation. This technology has been extensively studied by authors' research group since a first promising solution for linear actuators with single rod cylinders has been introduced by Rahmfeld and Ivantysynova in 1998. The main advantage of DC actuation is that metering losses are completely eliminated. This is achieved by removing the proportional valves controlling each actuator and installing a variable displacement pump per actuator. This allows controlling the actuator motion by controlling the pump displacement.

This manuscript was received on 25 May 2012 and was accepted after revision for publication on 15 December 2012

Previous work of the authors research group has demonstrated that this technology can achieve up to 50 % energy savings when compared to the conventional load sensing (LS) systems of the same machine (Zimmerman, Busquets and Ivantysynova, 2011). DC actuation not only eliminates metering losses but also allows utilization of potential and kinetic energy in aiding load mode of the actuator, i.e. energy from the actuator can be transferred in mechanical energy of the pump shaft while the pump runs in motoring mode. Without adding a storage devise to the system the recovered load energy needs to be used simultaneously by other machine drives. The elimination of metering losses in DC systems leads automatically to lower heat generation. The question to be answered is how much cooling power needs to be installed in DC multi-actuator machines?

For the investigation of DC actuation cooling requirements in mobile multi actuator DC machines, a Bobcat 435 hydraulic excavator has been equipped with DC actuation as part of a project funded by the Center for Compact and Efficient Fluid Power (CCEFP). A study of this machine conducted in 2010

by the authors' research group resulted in 50 % reduction of the cooling power requirement while maintaining acceptable working temperatures (Zimmerman, Busquets and Ivantysynova, 2011). In this previous study, the hydraulic fluid temperature was assumed to be the same throughout the system, while considering each component heat transfer individually. Good agreement was found in the steady state operation of the measured data of the hydraulic cooler; however, no comparison between the other hydraulic component temperatures was made. This paper will introduce a new approach for modeling the thermodynamic behavior of each of the hydraulic components of the closed circuit displacement controlled machine system. A set of mathematical models has been developed based on conservation of mass and energy to predict the temperature of the hydraulic oil in the entire system.

2 Excavator Hydraulic Circuit and Sensors

A simplified hydraulic circuit of the DC excavator including the installed sensors is shown in Fig. 1. For this simulation, the engine speed n_e, hydraulic actuators pressures p_A and p_B, and their corresponding hydraulic pumps pressures p_1 and p_2, and all swash plate angles $\beta_{pump,\ i}$, were measured. The low system pressure p_{lp}, and accumulator pressure p_{cp} were monitored. It should be noted that the low pressure accumulator is introduced in multi-actuator DC systems in order to keep the required charge pump size small. The unequal flow due to the area ratio of the single rod cylinders is balanced on the low pressure side of the systems. i.e. all low pressure lines are connected to the a singe charge pump and low pressure accumulator. The ambient and hood temperatures T_{amb} and T_{hood} respectively, were also measured and used in simulation to calculate the rejected heat. Finally, 16 thermocouples were installed to validate the simulated results through measured component temperatures.

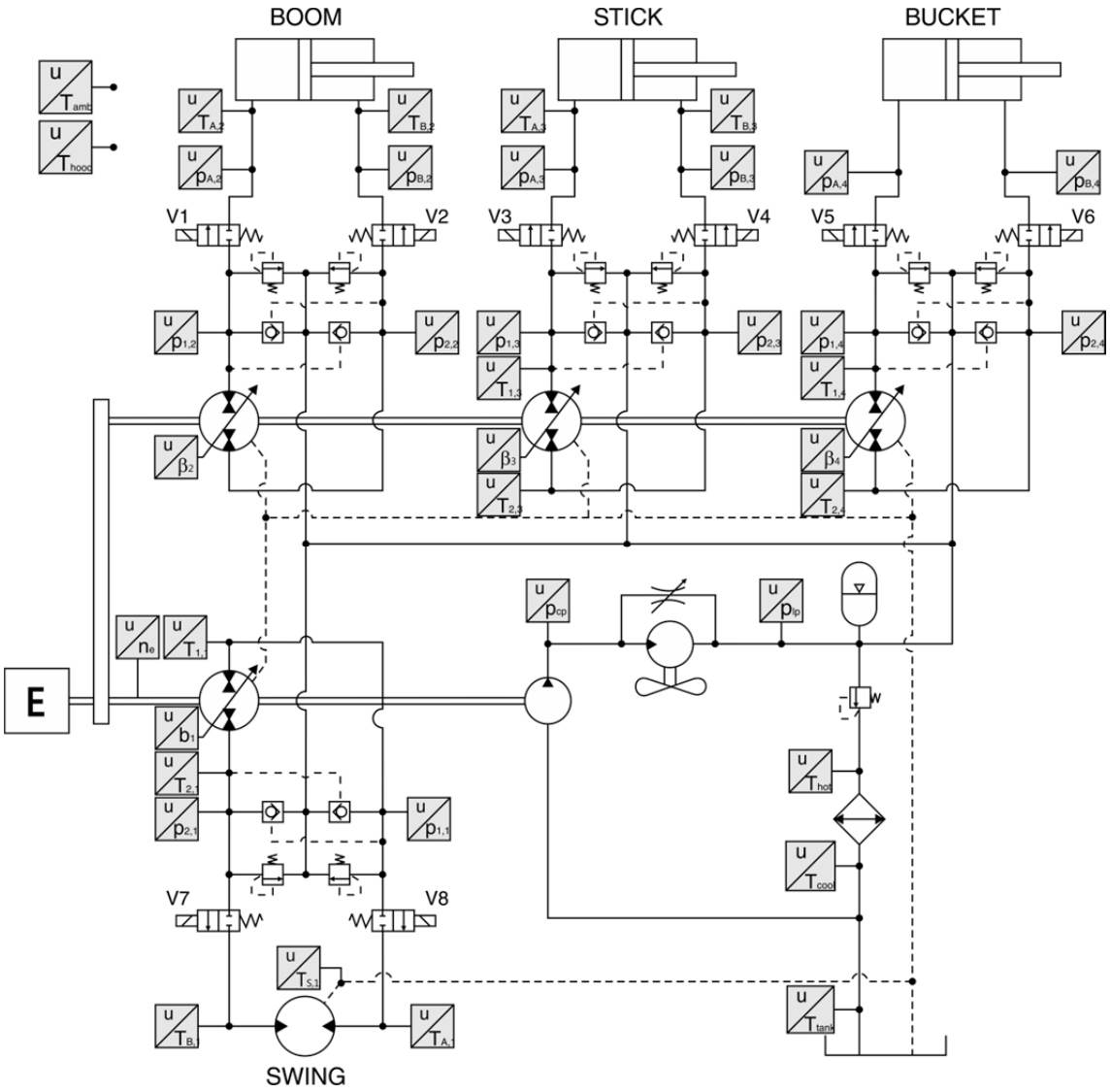

Fig. 1: *DC excavator hydraulic system and installed sensors*

3 System Measurements

A 45 min digging cycle was measured using the excavator. The digging cycle consisted of the operator removing dirt from directly in front of the machine and then rotating between 60 to 90 degrees to dump the dirt in a pile next to the hole being dug. The dirt in the field had not been dug before and due to weather conditions it was naturally compacted. Figure 2 shows a top view of the cycle.

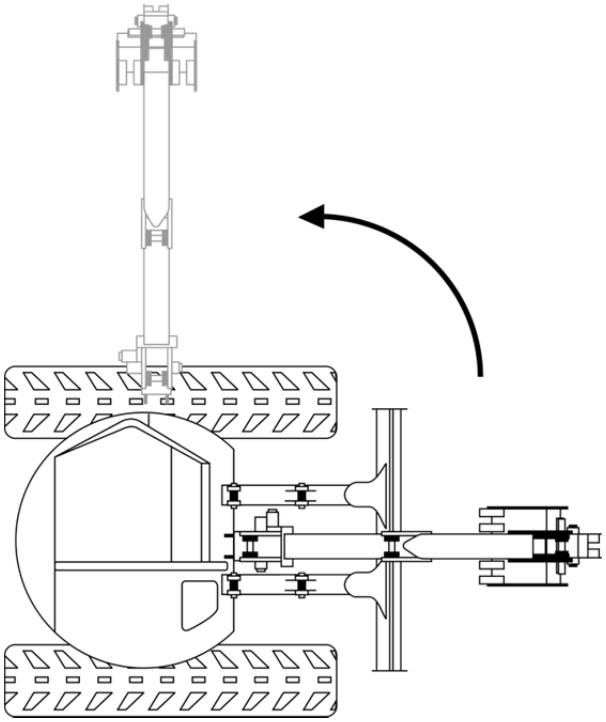

Fig. 2: *Top view of the digging cycle*

4 Thermodynamic System Analysis

The complex hydraulic architecture has been discretized into the different components, which significantly contribute to the thermal effects. The basic thermodynamic approach for each hydraulic component is represented in Fig. 3.

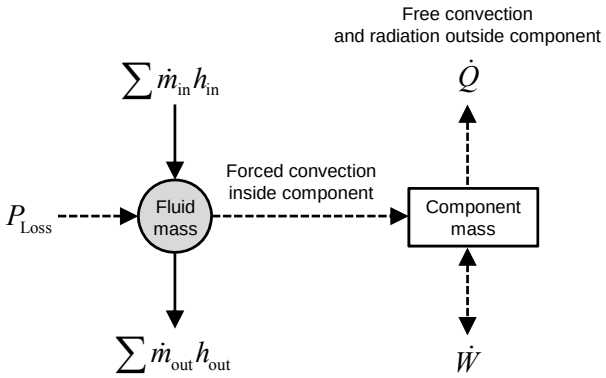

Fig. 3: *Individual components thermal model structure*

According to Fig. 3, it is assumed that the power losses P_{Loss} in each hydraulic component are converted to heat. Also, the heat transfer, work and fluid properties are calculated for each hydraulic component in the system.

4.1 Individual Heat Transfer Calculation

An essential aspect of this simulation is the heat rejected by each of the hydraulic components. For this reason, a set of heat transfer and thermo-dynamic relations was developed. As shown in Fig. 4, it was assumed that all components experienced forced convection from the oil temperature T_{oil}, to the inner wall A_i, of the material, then conduction through the component wall, and finally free convection to the air from the outer wall A_o, of the component. The majority of the excavator hydraulics are located under a hood within the excavator, for this reason an additional temperature sensor was installed to obtain those components surrounding temperature. It should also be noted that the assumption of free convection for the components is a conservative one since the cooling fan actually blows air throughout the hydraulic components located under the hood. The temperature entering each hydraulic component was obtained according to the hydraulic circuit depicted in Fig. 1.

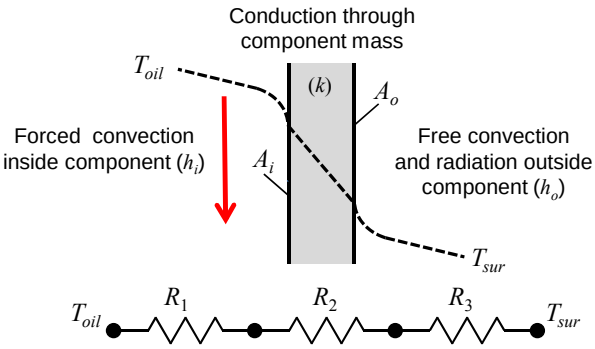

Fig. 4: *Heat transfer due to forced convection, conduction, and free convection*

An equivalent thermal resistance, R_{eq}, encompassing forced convection, conduction, free convection and radiation in series was derived for each component. Also, simple geometries such as pipes and cubes were assumed for the components geometries. Each of the thermal resistances can be expressed in terms of the inner and outer heat transfer coefficients $h_{con,\ in}$ and $h_{con,\ out}$ and the components inner and outer diameters d_i and d_o as:

$$
\begin{aligned}
&R_{eq} = R_1 + R_2 + R_3 \\
&R_1 = \frac{1}{h_{con,\ in} A_i} \quad \text{forced convection} \\
&R_2 = \begin{cases} \dfrac{\ln(d_o/d_i)}{2\pi L_{pipe} k} & \text{pipe conduction} \\ \dfrac{L_w}{ka^2} & \text{cube conduction} \end{cases} \\
&R_3 = \frac{1}{h_{con,\ out} A_o} + \frac{1-\varepsilon}{\varepsilon A_o} \quad \text{free convection and radiation}
\end{aligned}
\tag{1}
$$

Each of the cube side's conduction in Eq. 1 is calculated as a flat plane. Here L_w wall thickness, and a is

the side length of the cube shaped modeled components, such as the hydraulic reservoir and hydraulic valves. For the calculation of the pipe conduction L_{pipe} is the pipe length. The inner and outer convection coefficients $h_{con,\ in}$ and $h_{con,\ out}$ can be calculated with the Nusselt number from Table1.

It is important to mention that the thermal conductivity for different materials was taken into account (e.g. the reservoir thermal conductivity was that of plastic, 0.47 W/(m°K), while that of the pumps was steel, 43 W/(m°K)). Finally, ε in R_3 is the surface emissivity assumed to be 0.2. Then, the total heat transfer q, with conduction, convection and radiation is:

$$q = \frac{T_{oil} - T_{sur}}{R_{eq}} \tag{2}$$

Table 1: Calculation of Nusselt number for convection (Source: Rahmfeld, 2002 and VDI Heat Atlas)

Dimensionless parameters (l_c = characteristic length)	
Nusselt: $\mathrm{Nu} = \frac{k_{con} \cdot l_c}{k_f}$	Prandtl: $\mathrm{Pr} = \frac{\rho \cdot \nu \cdot c_p}{k_f}$
Reynolds: $\mathrm{Re} = \frac{v \cdot D_H}{\nu}$	Grashof: $\mathrm{Gr} = \frac{g \cdot l_c^3 \cdot \beta_{air} \cdot \Delta T}{\nu^2}$
Forced convection in pipe (physical characteristics at oil temperature, T_{oil})	
Laminar: $l_c = d_i$, $\mathrm{Pr_w} = \mathrm{Pr}(T_w)$, $\mathrm{Re} < 2300$ $\mathrm{Nu} = \left(3.66^3 + 0.7^3 + \left[1.615\sqrt[3]{\mathrm{Re}\cdot\mathrm{Pr}\cdot d_i / L} - 0.7\right]^3\right)^{1/3} \left(\frac{\mathrm{Pr}}{\mathrm{Pr_w}}\right)^{0.11}$	
Turbulent: $l_c = d_i$, $\mathrm{Pr}_w = \mathrm{Pr}(T_w)$, $d_i/l_c < 1$ $\mathrm{Nu} = \frac{\frac{(\mathrm{Re}-1000)\mathrm{Pr}}{8(1.82\log(\mathrm{Re})-1.64)^2}\left[1+\left(\frac{d_i}{L}\right)^{2/3}\right]}{1+12.7(\mathrm{Pr}^{2/3}-1)\sqrt{0.125(1.82\log(\mathrm{Re})-1.64)^{-2}}} \left(\frac{\mathrm{Pr}}{\mathrm{Pr_w}}\right)^{0.11}$	
Free convection to air (physical characteristics at $0.5(T_w+T_{sur})$)	
Horizontal cylinder: $\mathrm{Gr} = \mathrm{Gr}(T_w - T_{sur})$, $l_c = d_o$ $\mathrm{Nu} = \left(0.6 + 0.387\left[\mathrm{Gr}\cdot\mathrm{Pr}\left(1+\left(\frac{0.559}{\mathrm{Pr}}\right)^{9/16}\right)^{-16/9}\right]^{1/6}\right)^2$	
Cube: $\mathrm{Gr} = \mathrm{Gr}(T_w - T_{sur})$, $l_c = A_o^2/(4\cdot a^3)$ $\mathrm{Nu} = 5.748 + 0.752\left(\frac{\mathrm{Pr}\cdot\mathrm{Gr}}{\left[1-\left(\frac{0.492}{\mathrm{Pr}}\right)^{9/16}\right]^{16/9}}\right)^{0.252}$	

To calculate the required wall temperatures, heat transfer by radiation was neglected. This assumption is rather conservative but reasonable since within the range of operating temperatures of the system, the heat rejected through radiation is negligible. It was also assumed that both the inner and outer wall temperatures are equal. These assumptions greatly simplify the wall temperature calculation, ultimately leading to:

$$T_w = \frac{T_{oil} + T_{sur}\dfrac{\sum A_o \cdot k_{con,\ out}}{\sum A_i \cdot k_{con,\ in}}}{1 + \dfrac{\sum A_o \cdot k_{con,\ out}}{\sum A_i \cdot k_{con,\ in}}} \tag{3}$$

As mentioned before, for the calculation of the wall temperature, the heat rejected by radiation is neglected for simplification purposes, assuming a single wall temperature for the inner and outer faces. However, for completeness the total heat rejected includes radiative heat transfer as noted in Eq. (1).

4.2 Thermal Properties

All material and fluid properties were obtained in simulation based on both measured and simulated parameters. Thermal properties for the conduction of steel, the specific heat of steel, the conductivity of oil, air kinematic viscosity, air density, air specific heat, air thermal conductivity, and the air volumetric expansion coefficient were taken from tabulated data as a function of temperature from Incropera (2002). Measurement data for HLP 32 mineral oil (shown in Fig. 5) obtained by Flucon GmbH and published by Opperman (2007) was used to find the density of the oil as a function of pressure and temperature.

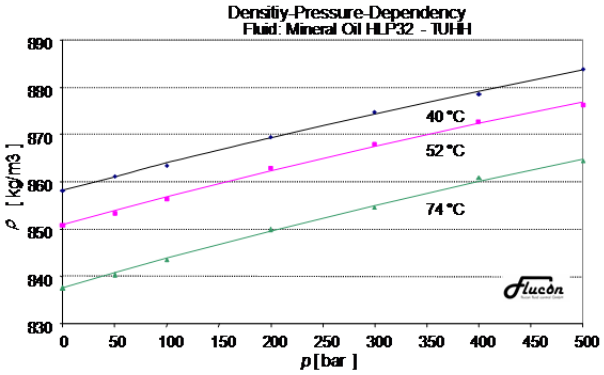

Fig. 5: *Pressure and temperature dependency of HLP32 mineral oil (Opperman, 2007)*

The viscosity of the oil was obtained using an expression similar to the empirical model in Eq. (5):

$$\mu = \mu_o \exp\left\{\ln\left(\frac{\mu_o}{\mu_r}\right)\left[\left(1+\frac{p}{p_r}\right)^z\left(\frac{T_o + 135°C}{T + 135°C}\right)^s - 1\right]\right\} \tag{4}$$

In Eq. (5), p_r and μ_r are a reference pressure and viscosity and T_o is the temperature at which the viscosity is μo at pressure $p = 0$. Also, the dimensionless pressure index is z and the temperature index is s (Pascovici, et. al 2001).

The specific heat of HLP32 mineral oil was obtained using the following equation (Oppermann, 2007) based on Grosse (1962) and Schilling (1985).

$$c_p(T) = c_0 + \alpha_c \cdot (T - 273.15)$$

with

$$c_0 = 1807\left[\frac{J}{kg\cdot K}\right] \text{ and } \alpha_c = 4.21\left[\frac{J}{kg\cdot K^2}\right] \tag{5}$$

Finally, the hydraulic oil enthalpy was determined using measured data (Oppermann, 2007) dependent on pressure and temperature.

4.3 Basis for Thermodynamic Approach

The one-dimensional form of the dynamic continuity equation is

$$\frac{dm}{dt} = \dot{m}_{\text{in}} - \dot{m}_{out} \tag{6}$$

Knowing that the density can be expressed as $\rho = m/V$, the continuity equation in terms of density becomes

$$\frac{d\rho}{dt} = \frac{dm/dt - \rho \cdot dV/dt}{V} \tag{79}$$

Since the fluid density describes a thermodynamic property, it can be expressed in terms of two other thermodynamic properties such as pressure and temperature. Then, the continuity equation (7) can be reformulated in terms of the pressure derivative.

$$\frac{dp}{dt} = \left.\frac{\partial p}{\partial \rho}\right|_T \frac{d\rho}{dt} + \left.\frac{\partial p}{\partial T}\right|_\rho \frac{dT}{dt} \tag{8}$$

Using the definition of the bulk modulus, $K = \rho \partial p/\partial \rho|_T$, combining Eq. (6) and Eq. (7) and substituting into Eq. (8), we obtain:

$$\frac{dp}{dt} = \frac{K \cdot \left[\left(\dot{m}_{in} - \dot{m}_{out}\right) - \rho \cdot dV/dt\right]}{\rho \cdot V} + \left.\frac{\partial p}{\partial T}\right|_\rho \frac{dT}{dt} \tag{9}$$

It can be observed that the $\rho \cdot dV/dt$ term in Eq. 10 accounts for moving boundaries. For this study, the moving boundaries term is only utilized in the control volumes describing the actuator chambers as their fluid volume changes several times during the digging cycle. This term will be carried out throughout the derivation and will then be simplified for those hydraulic components, which don't require such term.

By definition, the last term, $\partial p/\partial T|_\rho$, can be replaced by $\partial p/\partial T|_\nu$. Also, $\partial p/\partial T|_\rho = \beta/x_{\text{T}}$ where β is the coefficient of cubic expansion and x_{T} is the isothermal compressibility. Furthermore, the bulk modulus is the reciprocal of x_{T}. Substituting the previous relations into Eq. (9) gives

$$\frac{dp}{dt} = \frac{K \cdot \left[\left(\dot{m}_{\text{in}} - \dot{m}_{\text{out}}\right) - \rho \cdot dV/dt\right]}{\rho \cdot V} + \beta \cdot K \cdot \frac{dT}{dt} \tag{10}$$

The differential equation describing the energy of a control volume in which potential and kinetic energies have been neglected can be expressed as

$$\frac{dE}{dt} = \sum \dot{m}_{\text{in}} \cdot h_{\text{in}} - \sum \dot{m}_{\text{out}} \cdot h_{\text{out}} + \dot{Q} - \dot{W} \tag{11}$$

This may be rearranged in terms of enthalpy as an intensive property

$$\frac{dh}{dt} = \frac{1}{\rho \cdot V}\left[\sum \dot{m}_{\text{in}} \cdot h_{\text{in}} - \sum \dot{m}_{\text{out}} \cdot h_{\text{out}} + \dot{Q} - \dot{W} + V \cdot \frac{dp}{dt}\right] \tag{12}$$

For some hydraulic components, Eq. (12) can be further simplified if the flow into and out of the control volume is equal. To find a more generalized form, the derivation will be carried out assuming that such flows are not equal and further simplification will be performed in Section 5 where each of the hydraulic components is described.

To convert the enthalpy derivative to that of temperature, the following relationship between thermodynamic properties is utilized as a basis:

$$\frac{dh}{dt} = \left.\frac{\partial h}{\partial p}\right|_T \frac{dp}{dt} + \left.\frac{\partial h}{\partial T}\right|_p \frac{dT}{dt} \tag{13}$$

By using equations Eq. (12) and Eq. (13) and solving for the temperature derivative gives

$$\begin{aligned}\frac{dT}{dt} = & \frac{1}{\left.\frac{\partial h}{\partial T}\right|_p \cdot \rho \cdot V} \\ & \left[\sum \dot{m}_{\text{in}} \cdot h_{\text{in}} - \sum \dot{m}_{\text{out}} \cdot h_{\text{out}} + \dot{Q} - \dot{W} + V \cdot \frac{dp}{dt}\right] \\ & - \frac{1}{\left.\frac{\partial h}{\partial T}\right|_p} \cdot \left(\left.\frac{\partial h}{\partial p}\right|_T \cdot \frac{dp}{dt}\right)\end{aligned} \tag{14}$$

Using $c_{\text{p}} = \partial h/\partial T|_p$ for specific heat with $\partial h/\partial p|_T = 1/\rho - \beta \cdot T \cdot v$, and simplifying yields

$$\begin{aligned}\frac{dT}{dt} = & \frac{1}{\rho \cdot c_{\text{p}} \cdot V}\left[\sum \dot{m}_{\text{in}} \cdot h_{\text{in}} - \sum \dot{m}_{\text{out}} \cdot h_{\text{out}} + \dot{Q} - \dot{W}\right] \\ & + \frac{v \cdot \beta \cdot T}{c_{\text{p}}} \cdot \frac{dp}{dt}\end{aligned} \tag{15}$$

Coupling Eq. (10) and Eq. (15) and simplifying gives a complete formulation for the temperature calculation of the control volume. In some instances, it may be more affordable computationally to further simplify the enthalpy expression by making use of the oil specific heat and the differential temperature in the control volume.

4.4 Hydraulic Pump Model

Referring to Fig. 1, the DC excavator system has four variable displacement pumps. The system was designed such that there are no additional travel pumps idling since two of the cylinders are shut off when travel is required and the pump flows are diverted to the travel motors.

The pump control volume was divided in two smaller control volumes, V_{I} and V_{II} to obtain both the temperature leaving the pump and the pump case drain temperature. Figure 6 shows the basic approach for the pump temperature calculation. In this case, node m_{A}, m_{B} and m_{C} represent the fluid mass inside the pump side A, side B and case drain respectively. Also, Q_1 and Q_2 are the flows into and out of the first control volume V_{I}, and Q_{s} is the case drain flow. To calculate the heat transfer, the hydraulic pumps were regarded as 15 cm long steel pipes with 15 cm in outer diameter and 10 cm in inner diameter. These calculations were performed for the first control volume V_{I}, assuming no energy exchange by means of heat rejection or work is possible in the second control volume V_{II}.

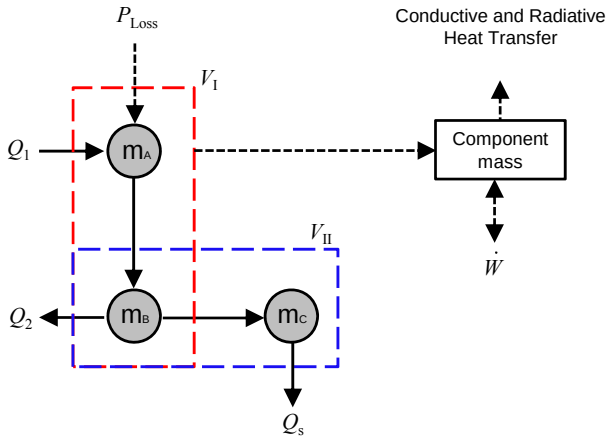

Fig. 6: *Basic thermodynamic approach for pump temperature calculation*

Due to the size of the hydraulic pumps, the transient thermal response occurs significantly faster than that of components which hydraulic fluid capacity is greater such as the reservoir. Referring to Fig. 6, the temperature leaving the pump T_2, and the pump case drain temperature T_C, can be calculated by Eq. (16) and Eq. (17) respectively. It is important to mention that no boundary work is done in this system; therefore, the effects of the *dp/dt* term in Eq. (15) can be neglected.

$$\frac{dT_2}{dt} = \frac{1}{\rho \cdot c_p \cdot V} \cdot \left[\sum \dot{m}_A \cdot h_A - \sum \dot{m}_B \cdot h_B + \dot{Q} - \dot{W}_{pump} \right] \quad (16)$$

$$\frac{dT_C}{dt} = \frac{1}{\rho \cdot c_p \cdot V} \cdot \left[\sum \dot{m}_B h_B - \sum \dot{m}_C h_C \right] \quad (17)$$

4.5 Fan and Charge Pump Model

Due to the small displacement volumes of both the charge pump (14.1 cc/rev) and the fan drive (8 cc/rev) and the challenges posed by the existence of a proportional valve, which is temperature dependent, influencing the pressure at the fan drive, it was decided to join these two hydraulic components into a single control volume called fan system. Since measurements exist for the pump speed and the pressure after the charge pump and knowing that it gets flow from the reservoir which is nearly at atmospheric pressure, the charge pump flow and torque were calculated using catalogue data. Although measurements also exist for the pressures across the fan drive, it is not possible to calculate the work done by the fan drive due to the influence of the already mentioned proportional valve. The solution to this was to directly measure the fan drive shaft speed using an optical sensor. Then, the total work in the fan-charge pump system, $\dot{W}_{fcps}$, can be expressed as:

$$\dot{W}_{fcps} = M_{cp} n_{cp} - M_{fan} n_{fan} \quad (18)$$

Since the charge pump is a gear pump with no case drain line, assuming the leakage from the fan motor is negligible and neglecting the moving boundaries part of the equation, the continuity relationship described in Eq. (10) could be solved. Combining Eq. (15), (10) and (18) and providing a proper formulation for the heat transfer gives a relation for the temperature calculation in the fan system, T_{fs}. To properly account for the heat rejected in this control volume, both the charge pump and the fan motor were regarded as 10 cm long steel pipes which outer and inner diameters are 10 cm and 8 cm respectively.

$$\frac{dT_{fcps}}{dt} = \frac{1}{\rho \cdot V \cdot \left(c_p - \beta^2 \cdot T \cdot K \right)} \cdot \left[\sum \dot{m}_{in} \cdot h_{in} - \sum \dot{m}_{out} \cdot h_{out} + \dot{Q} - \dot{W}_{fcps} \right] + \frac{\beta \cdot T \cdot K \left(\dot{m}_{in} - \dot{m}_{out} \right)}{\rho \cdot \left(c_p - \beta^2 \cdot T \cdot K \right)} \quad (19)$$

4.6 Slew Motor Model

Similar to the charge pump, the speed and pressure across the hydraulic motor of the slew drive is measured and the work done by the slew motor can be expressed by multiplying the motor torque, M_{slew}, and its shaft speed n_{slew}:

$$\dot{W}_{slew} = M_{slew} \cdot n_{slew} \quad (20)$$

The flow calculation of the slew motor is based on the speed of the engine and the speed of the slew motor. Also, the leakage flow was approximated using catalogue data of mean values dependent upon pressure and speed. The slew motor temperature derivative, dT_{slew}/dt, can then be expressed similar to that of the hydraulic pumps. Also the leakage temperature was obtained using the same basic approach described in Fig. 6. Finally, the heat rejected by the slew motor was calculated assuming this component is a 25 cm long steel pipe with 25 cm and 20 cm in outer and inner diameters respectively.

$$\frac{dT_{slew}}{dt} = \frac{1}{\rho \cdot c_p \cdot V} \cdot \left[\sum \dot{m}_A \cdot h_A - \sum \dot{m}_B \cdot h_B + \dot{Q} - \dot{W}_{slew} \right] \quad (21)$$

$$\frac{dT_{sc}}{dt} = \frac{1}{\rho \cdot c_p \cdot V} \cdot \left[\sum \dot{m}_B \cdot h_B - \sum \dot{m}_C \cdot h_C \right] \quad (22)$$

4.7 Hydraulic Cooler Model

An accurate model of the hydraulic cooler is essential to the thermal model of the excavator system because this is where most of the heat from the system is rejected. For this reason an empirical model of the cooler was used. The heat rejected by the cooler can be calculated by:

$$\dot{Q}_{cooler} = k_{con} \cdot A_{cooler} \cdot \left(T_{oil} - T_{sur} \right) \quad (23)$$

The hydraulic cooler is finned tubing and is cooled by fan driven air. The surface area was calculated as the area of all fins and tubing to be 3.46 m^2. Also, the flow rate through the cooler is:

$$Q_{cooler} = Q_{cp} - Q_{lp} - \dot{V}_{oil,\,accu} \quad (24)$$

where

$$Q_{\mathrm{cp}} = \eta_{\mathrm{V}} \cdot n_{\mathrm{cp}} \cdot \frac{V_{\mathrm{d,\,cp}}}{2\pi}$$
$$Q_{\mathrm{lp}} = \sum\left(Q_{\mathrm{A,\,i}} - Q_{\mathrm{B,\,i}}\right) + \sum Q_{\mathrm{s,\,i}} \qquad (25)$$
$$V_{\mathrm{oil,\,accu}} = V_{\mathrm{o}} \cdot \left(1 - \left(\frac{p_{\mathrm{o}}}{p_{\mathrm{lp}}}\right)^{1/n}\right)$$

In the above expression Q_{A} is defined as the flow into the bore side of the cylinders and Q_{B} is defined as the flow out of the rod side of the cylinders and it is the difference between these flows plus the volumetric losses of the actuators Q_{s} which must be balanced by the low pressure flow. Also Q_{cp} and Q_{lp} are the charge pump and the low pressure flows respectively, Finally, η_{V} is the volumetric efficiency of the charge pump, n_{cp} is the charge pump shaft speed, $V_{\mathrm{d,\,cp}}$ is the charge pump displacement and $V_{\mathrm{oil,\,accu}}$ is the rate of change of the accumulator oil volume.

To create a model of the hydraulic cooler, measurements were made on the excavator while idling with no actuators in use. This means that the accumulator volume will be constant and there will be no low pressure flow. Using Eq. (24) the cooler flow rate will be equal to the charge pump flow rate. Measurements of the pressure drop across the cooling fan hydraulic motor, p_{cp} - p_{lp}, the temperature drop across the cooler, T_{hot} - T_{cool} as indicated in Fig. 1, and the engine speed, n_{e}, were taken at several different engine idle speeds to allow for a range of flow rates through the cooler and a range of pressure drops across the cooling fan motor (the pressure drops correspond to steady state fan speeds). Equation (23) was used to calculate the actual heat rejected by the cooler during the measurements and the coefficients a and b in Eq. (26) were regressed to create a linear model of the cooler as a function of the normalized pressure drop across the hydraulic fan motor and the normalized oil flow through the cooler.

$$k_{\mathrm{cool}} = a \cdot \left(\frac{p_{\mathrm{cp}} - p_{\mathrm{lp}}}{15\mathrm{e}5\ \mathrm{Pa}}\right) + b \cdot \left(\frac{Q_{\mathrm{cooler}}}{5.54 \times 10^{4}\ \mathrm{m^3/s}}\right) \qquad (26)$$

The resulting coefficients for the model were 34.1 W/K and 96.9 W/K for a and b respectively. This resulted in a value of $k_{\mathrm{cool}} = 4.95 \times 10^4$ W/(m^2·°C)/(m^3/s) giving an average value for the convection coefficient to be $k_{\mathrm{con}} \approx 43$ W/(m^2·°C). This value seems reasonable considering typical convection coefficients for finned tube heat exchangers with water in the tube and air in the cross flow are between 25 and 50 W/(m^2·°C). (Incropera and Dewitt, 2002). The heat rejected also lies within the range specified by the product catalogue. Therefore, the average value used in the model is consistent with the measured values. To validate the model Fig. 7 shows a plot of measured and modeled q_{cool} during a working cycle of the excavator.

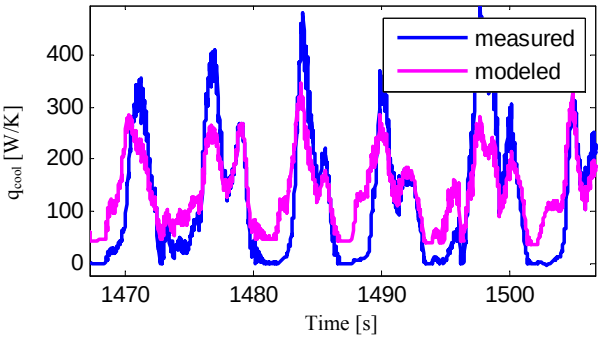

Fig. 7: *Comparison of measured and modeled oil cooler power during digging cycle*

4.8 Hydraulic Line Model

The temperature of the various hydraulic lines is calculated using Eq. (10) and (15). The assumptions for these control volumes include no work either in or out of the system and constant volume. Therefore, heat transfer is the only aspect influencing the fluid temperature calculation. It is important to mention that only metallic pipes were modeled, assuming the heat transfer contribution from the rubber hydraulic lines is negligible due to the low thermal conductivity of rubber. Each of the two modeled lines dimensions are 100 cm long with outer and inner diameters of 2 cm and 11.7 cm respectively. Finally, by assuming that the mass flow into and out of the control volume are equal, the temperature derivative can then be reduced to:

$$\frac{dT_{\mathrm{line}}}{dt} = \frac{1}{\rho \cdot V \cdot \left(c_{\mathrm{p}} - v \cdot \beta^2 \cdot T \cdot K\right)} \cdot \left[\dot{m}_{\mathrm{e}} \cdot \left(h_{\mathrm{in}} - h_{\mathrm{out}}\right) - \dot{Q}\right] \qquad (27)$$

It is important to note that the moving boundaries term has been eliminated in Eq. (27) due to the constant volume assumption.

4.9 Accumulator Model

The accumulator in this system is a 4-liter low pressure accumulator with a pressure pre-charge of 7 bar. The flow rate into the accumulator is dependent upon the actuators motion, the charge pump flow and the low pressure setting. The actuator work can be calculated as:

$$\dot{W}_{\mathrm{accu}} = p \cdot \frac{dV}{dt} \qquad (28)$$

The accumulator temperature derivative requires both Eq. (10) and (15). To accurately calculate the accumulator temperature, the pressure derivative term in Eq. (10) must account for moving boundaries. Then, the temperature derivative for the accumulator is defined by:

$$\frac{dT_{\mathrm{accu}}}{dt} = \frac{1}{\rho \cdot V \cdot \left(c_{\mathrm{p}} - \beta^2 \cdot T \cdot K\right)} \left[\sum \dot{m}_{\mathrm{e}} \cdot h_{\mathrm{e}} - \sum \dot{m}_{\mathrm{l}} \cdot h_{\mathrm{l}} + \dot{Q} - \dot{W}_{\mathrm{accu}}\right] + \frac{\beta \cdot T \cdot K}{c_{\mathrm{p}} - \beta^2 \cdot T \cdot K} \cdot \left(\frac{\left(\dot{m}_{\mathrm{e}} - \dot{m}_{\mathrm{l}}\right)}{\rho} - \frac{dV}{dt}\right) \qquad (29)$$

An alternative to Eq. (30) is to differentiate the measured pressure and utilize Eq. (16). The volume, V, in Eq. (30) can be calculated using an adiabatic relation with n = 1.25. Also, the accumulator was regarded as a steel pipe, 60 cm long, 20 cm in outer diameter and 18.5 cm in inner diameter.

4.10 Linear Actuator Model

Figure 8 shows a schematic of the linear actuator with the two temperature calculations obtained by the model, each describing a different actuator chamber. The actuator work can be expressed similar to Eq. (28). Positive work indicates work being done into the system and negative work indicates work done by the system. It can be observed that as the cylinder extends, work is negative in chamber A and positive in chamber B. Opposite motion has the opposite effect in the work calculation. Heat rejected through the cylinder walls was also calculated for each of the cylinder chambers accounting for the change in surface area as the actuator extends or retracts. It was assumed that there is no heat transfer between both chambers through the actuator piston as the transient temperature changes are rapid.

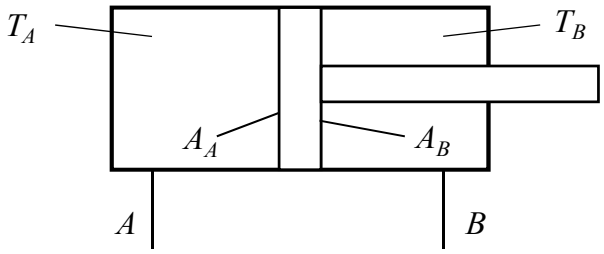

Fig. 8: *Linear actuator schematic*

Both Eq. (10) and Eq. (15) are combined to find the actuator chambers temperature derivative. In this case the effects of the *dp/dt* term, as well as the moving boundaries term, are of great importance in the accurate determination of the actuators temperature, Eq. 30 describes such relation.

Similar to the accumulator, each chamber volume, V, changes depending on the actuator motion. In this case the position of the actuator and their corresponding chamber inner areas were utilized to calculate the chambers volume. Since all three actuators have different dimensions, the calculation of the heat rejection will yield different values. The boom actuator for instance was regarded as a steel pipe with 11.5 cm in outer diameter and 9.5 cm in inner diameter. The arm actuator was also regarded as a steel pipe 10.5 cm in outer diameter and 8.5 cm in inner diameter. The bucket actuator was regarded as steel pipe as well, 8.5 cm in outer diameter and 6.5 cm in inner diameter. Finally, the position of each of the actuator determines the lengths the pipes.

4.11 Load Holding Valve Model

Cartridge valves (V1 to V8 on Fig. 1) are used for actuators load holding and/or shut off. The cartridge valves are mounted in a steel block in pairs. Similar to the hydraulic line model, the load holding valve model assumption is that no work is done and its volume remains constant. Hence, the only influence in the thermodynamic behavior of the hydraulic fluid is heat transfer, which is relatively large due to its large surface area and material. In this case, this component was regarded as a steel cube 15 cm in side length. Further, since the mass flow rates in and out of the system were assumed to be equal, the temperature derivative equation for the load holding valves can be reduced as follows:

$$\frac{dT_{\text{valve}}}{dt} = \frac{1}{\rho \cdot V \cdot \left(c_{\text{p}} - v \cdot \beta^2 \cdot T \cdot K\right) \cdot \left[\dot{m}_{\text{in}} \cdot \left(h_{\text{in}} - h_{\text{out}}\right) - \dot{Q}\right]} \tag{30}$$

Due to the constant volume assumption, the moving boundaries term has been disregarded from Eq. (30).

4.12 Reservoir Model

Unlike other hydraulic components, the pressure difference across the tank is negligible due to its open-to-atmosphere nature. Since no work is done in the tank, heat transfer is the only parameter affecting the thermodynamic behavior of the hydraulic fluid. In this case, such calculation is carried on assuming the hydraulic reservoir is a plastic cube which is hollow to contain the hydraulic oil. The assumed dimensions for each of the cube side lengths are 25cm. Then, Eq. (15) can be reduced to:

$$\frac{dT_{\text{res}}}{dt} = \frac{1}{\rho \cdot c_p \cdot V} \cdot \left[\dot{m}_{\text{in}} \cdot \left(h_{\text{in}} - h_{\text{out}}\right) - \dot{Q}\right] \tag{31}$$

5 Simulation Results

The thermodynamic behaviour of each hydraulic component was simulated for the given working cycle; when coupled together, they allow for the hydraulic fluid temperature prediction in the entire DC system. As shown in Fig. 9, the tank simulated temperature deviates from the measured temperature by almost 10°C. It is believed that this large deviation may have been caused by the model inability to account for energy previously stored in the tank since before measurements were recorded the machine had been driven to an outside location and the hydraulic oil temperature in the tank was much hotter. Although this is also true for the rest of the hydraulic components, the tank has the largest volume and its walls are plastic rather than steel like the rest, which slows heat rejection. This can be observed as the initial temperatures of the entire low pressure system shown in Fig. 9 are lower than that of the tank. Different initial conditions were given to attempt to account for such energy; however, the simulation stabilized every time at the same value.

From Fig. 9, it can also be observed that there is a very close agreement between the measured and simulated temperatures for both the inlet and outlet temperatures of the cooler. Finally, the high noise in the temperatures agree with the behaviour of the low pressure system as the volumes in the accumulator and tank constantly change, displacing oil from the asymmetric

actuators and charge pump which are at different temperatures. No measurements were obtained for the accumulator temperature or the charge pump temperature; however, the trends shown by the simulated data are very close to the expected temperatures.

Figure 10 shows a comparison between the simulated results and the measured temperatures of both the pump inlets and outlets. It can be observed that the temperatures of the swing pump are closely approximated by the model; however by the end of the cycle, the simulated temperature increases rapidly while the measured temperature increases at a slower rate. In this case such behaviour can be explained by the very small swing motor control volume. Therefore the temperature is more susceptible to changes in pressure and or speed. For this cycle, at time 2,500 s the engine speed was increased to its maximum while the rest of the cycle was measured at 90% of the maximum engine speed.

From Fig. 10, it can also be observed that although the general trend of the temperatures in the stick and bucket pumps is followed, those temperatures are too noisy. This may be due to the rapid changes in flow, since as shown in Fig. 1, the closed circuit pumps are connected to the low pressure to compensate for the differential volume of the single rod cylinders. In this case, when flow is required to compensate for the differential volume of the asymmetrical cylinders, oil from the low pressure line, which is at a lower temperature due to the cooler, is allowed to flow into the actuator. In actuality, this phenomenon occurs at a lower rate since the flows don't mix perfectly. In such case, a temperature increment of 5°C is possible even during a very short period of time.

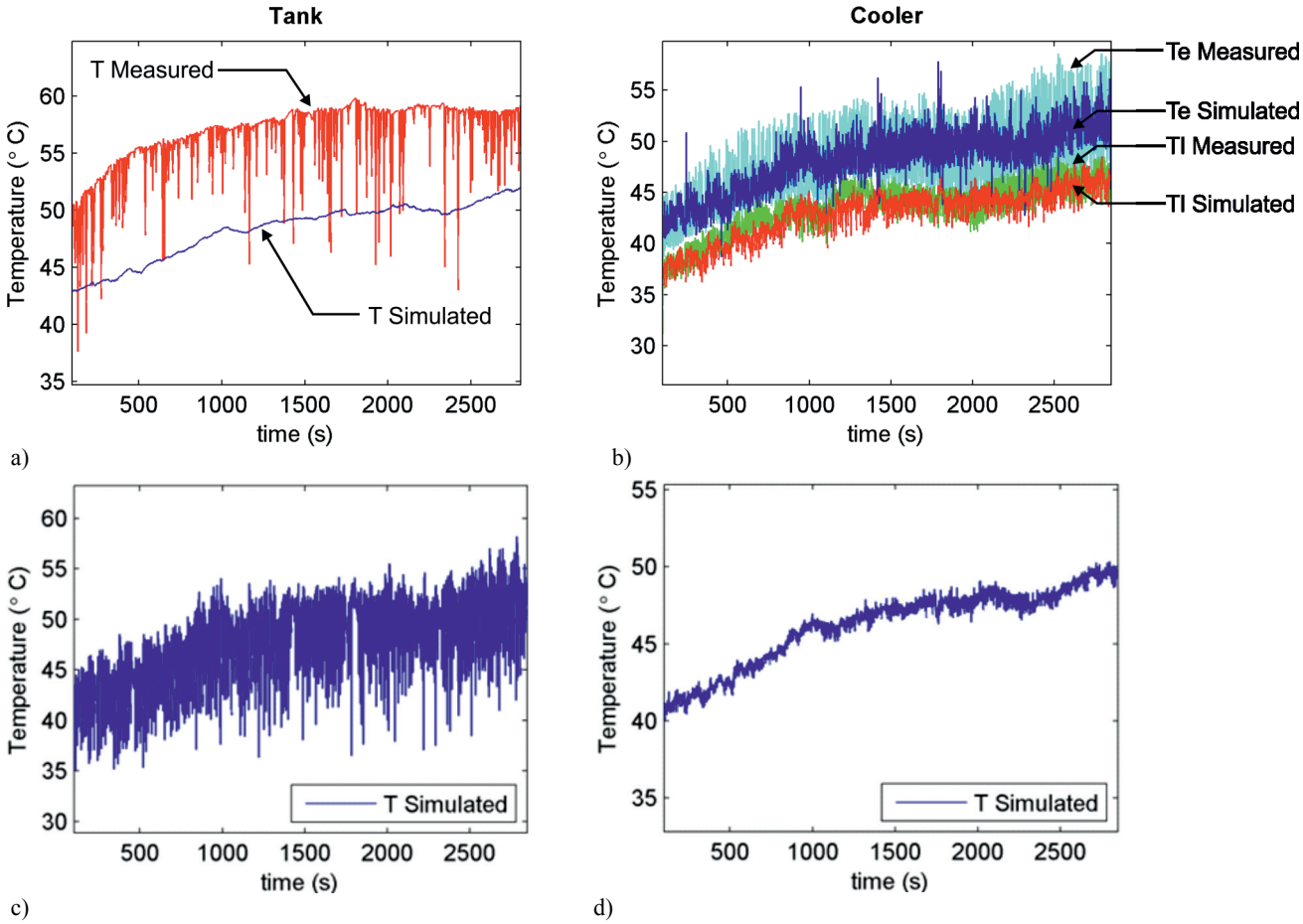

Fig. 9: *Low pressure system measured and simulated hydraulic fluid temperatures a) shows the tank simulated and measured temperatures, b) shows the simulated and measured cooler temperatures, c) shows the simulated accumulator temperature and d) shows the simulated charge pump temperature*

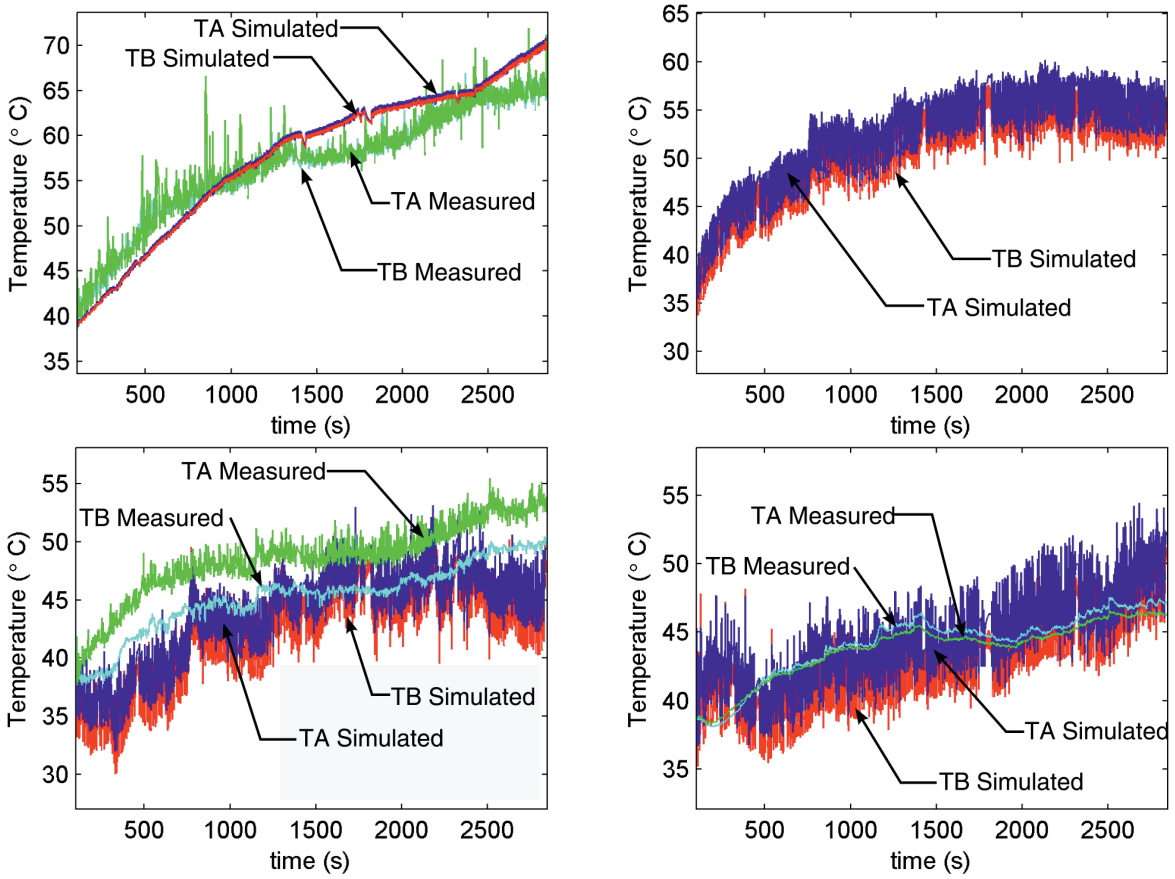

Fig. 10: *Pumps measured and simulated hydraulic fluid temperatures a) shows the slew motor pump simulated and measured temperatures, b) shows the boom pump simulated temperatures, c) shows the stick pump simulated and measured temperatures and d) shows the bucket pump simulated and measured temperatures*

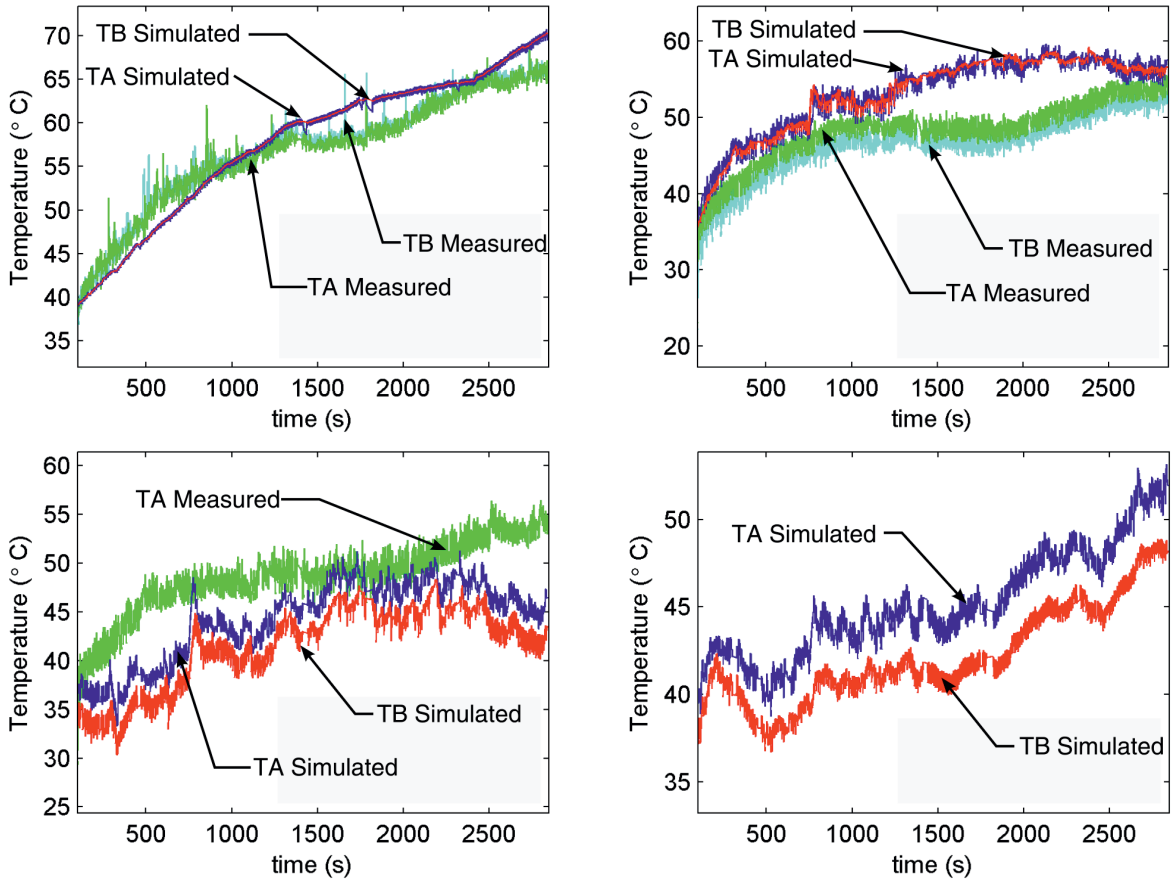

Fig. 11: *Actuators measured and simulated hydraulic fluid temperatures a) shows the slew motor simulated and measured temperatures, b) shows the boom actuator simulated temperatures, c) shows the stick actuator simulated and measured temperatures and d) shows the bucket pump simulated and measured temperatures*

No measurement data is available for the boom pump temperatures; however, a close comparison of these temperatures with the measured temperatures in the boom actuator can be made, these temperatures are shown in Fig. 11.

Figure 11 shows a comparison between the simulated and measured temperatures of the hydraulic oil in all four actuators. When comparing Fig. 10 to Fig. 11, it can be observed that the temperature trends of the actuators closely follow those of the pumps. It can also be observed that the temperatures in the swing and boom are approximated relatively well. However, the general temperature trend of the stick actuator is different when compared to the measured temperature. In this case, no measurements are available for the bucket actuator but an intiution of the trends which these temperatures should follow can be acquired by observing the measured pump temperatures in Fig. 10. The same follows with the B port of the stick cylinder.

6 Conclusions

A comprehensive thermal model of the excavator displacement controlled hydraulic system was developed to analyze the localized oil temperatures in the system. The simulated results show that the model is valid for the approximation of the thermal behavior of displacement controlled hydraulic systems. Furthermore, the temperature prediction shows that the localized temperatures in displacement controlled systems are within typical working temperatures for hydraulic systems in mobile applications. This mathematical model can also be utilized to analyze the cooling capacity requirements of displacement controlled systems to possibly reduce the cooler size. Future work will include the simulation of different hydraulic architectures such as larger excavators or other off highway vehicles to extend the validity of the model.

Nomenclature

A	Area	[m^2]
a	Cube side length	[m]
c_p	Specific heat	[kJ/(kg·^{o}C)]
D_H	Hydraulic diameter	[m]
d	Diameter	[m]
g	Gravity	[m/s^2]
Gr	Grashof number	[-]
h	Specific enthalpy	[Nm/kg]
K	Hydraulic oil bulk modulus	[bar]
k_{con}	Convection coefficient	[W/(m2·^{o}C)]
k	Conduction coefficient	[W/(m·^{o}C)]
k_f	Fluid heat transfer coefficient	[W/(m^2·^{o}C)/(m^3/s)]
M	Torque	[N·m]
m	Mass	[kg]
$\dot{m}$	Mass flow rate	[kg/s]
Nu	Nusselt number	[-]
n	Rotational speed	[rpm]
P	Power	[W]
Pr	Prandtl number	[-]
p	Pressure	[Pa]
Q	Flow rate	[m^3/s]
$\dot{Q}$	Rate of heat rejection	[W/s]
R	Thermal resistance	[(m2·^{o}C)/W]
Re	Reynolds number	[-]
T	Temperature	[^{o}C]
t	Time	[s]
V	Volume	[m^3]
v	Fluid velocity	[m/s]
W	Work	[W]
β	Volumetric thermal expansion	[1/^{o}K]
β_{pump}	Pump swash plate angle	[% of max]
μ	Viscosity	[Pa·s]
ν	Kinematic viscosity	[m^2/s]
ρ	Density	[kg/m^3]

Subscripts

A	Port A
accu	Accumulator
act	Actuator
air	Air
B	Port B
cool	Cooled oil
cooler	Hydraulic cooler
con	Convection
cp	Charge pump
e	engine
f	Fluid
fan	Fan motor
fcps	Fan and charge pump system
hot	Hot oil
i	Inner diameter and inner area
in	Flow, mass flow and enthalpy into the control volume
lp	Low pressure
o	Outer diameter and inner area
out	Flow, mass flow and enthalpy out of the control volume
oil	Hydraulic oil
pump	Hydraulic pump
res	Hydraulic reservoir
sc	Slew motor case
slew	Slew motor
sur	Surrounding
valve	Load holding valve
w	Wall

Acknowledgements

This research was supported by the Center for Compact and Efficient Fluid Power, a National Science Foundation Engineering Research Center funded under cooperative agreement number EEC-0540834.

References

Incropera, F. and **Dewitt, D.** 2002. *Fundamentals of Heat and Mass Transfer*. John Wiley and Sons, New York. p. 647.

Li Cheng-gong and **Jiao Zong-xia.** 2006. Thermal-hydraulic Modeling and Simulation of Piston Pump. *Chinese Journal of Aeronautics*. Volume 19, Issue 4. pp. 354 - 358.

Li, J., Zhang, X. and **Yin, Y.** 2011. Dynamic Temperature Simulation of an Accumulator in Aircraft Hydraulic Systems. *International Conference on Fluid Power and Mechatronics*. Beijing, China, pp. 653 - 657.

Li, Y., Su, X., Xu, H., and **Li, D.** 2008. Thermal-hydraulic modeling and simulation of high power hydro-motor. *7th International Conference on System Simulation and Scientific Computing*. 978-1-4244-1786-5.

Oppermann, M. 2007. A New Approach for Failure Prediction in Mobile Hydraulic Systems. VDI Fortschritt-Berichte. Reihe 12 No. 665. Düsseldorf: VDI. ISBN: 978-3-18-366512-9.

Pascovici, M. and **Khonsari, M.** 2001. Scuffing Failure of Hydrodynamic Bearings Due to an Abrasive Contaminant Partially Penetrated in the Bearing Over-Layer. *ASME Journal of Tribology*. Vol. 123. pp. 430 - 440.

Rahmfled, R. 2002. Development and Control of Energy Saving Hydraulic Servo Drives for Mobile Systems. VDI Fortschritt-Berichte. Reihe 12 No. 527. Düsseldorf: VDI. ISBN: 3-18-352712-X.

Sidders, J., **Tilley, D.** and **Chapple, P.** 1996. Thermal-hydraulic Performance Prediction in Fluid Power Systems. *Journal of Systems and Control Engineering*. Vol. 210. pp. 231 - 242.

VDI Heat Atlas. 2006. Tenth, revised and extended edition, Springer-Verlag Berlin Heidelberg.

Zimmerman, J., **Busquets, E.** and **Ivantysynova, M.** 2011. 40 % Fuel Savings by Displacement Control Leads to Lower Working Temperatures - A Simulation Study and Measurements. *Proceedings of the 52nd National Conference on Fluid Power 2011*, NCFP I11 - 27.2

Zimmerman, J. and **Ivantysynova, M.** 2010. Reduction of Engine and Cooling Power by Displacement Control. *Proc. of the 6th FPNI PhD Symposium*, West Lafayette, USA, pp. 339 - 352.

Enrique Busquets
received his B.S. degree in Mechanical Engineering from the University of Texas at El Paso in 2011. Since then he has worked as a graduate researcher/PhD student at Purdue University in the development of highly efficient displacement controlled systems for multi-actuator systems. His research interests include the thermal-hydraulic behavior analysis of hydraulic systems.

Monika Ivantysynova
Born on December 11th 1955 in Polenz (Germany). She received her MSc. Degree in Mechanical Engineering and her PhD. Degree in Fluid Power from the Slovak Technical University of Bratislava, Czechoslovakia. After 7 years in fluid power industry, she returned to university. In April 1996 she received a Professorship in fluid power & control at the University of Duisburg (Germany). From 1999 until August 2004 she was Professor of Mechatronic Systems at the Technical University of Hamburg-Harburg. Since August 2004 she is Professor in Mechanical Engineering and Agricultural and Biological Engineering at Purdue University, USA. She was approved as Maha named Professor in Fluid Power Systems and director of the Maha Fluid Power Research Center at Purdue University in November 2004. Her main research areas are energy saving actuator technology and model based optimization of displacement machines as well as modeling, simulation and testing of fluid power systems. Besides the book "Hydrostatic Pumps and Motors" published in German and English, she has published more than 90 papers in technical journals and at international conferences.